arXiv:2106.00338v1 [cond-mat.mes-hall] 1 Jun 2021

Theory of Chiral Transport in Carbon Nanotubes

Masaki Noro,† Junya Tanaka,† Takehito Yokoyama,† and Shuichi Murakami*,†,‡

†*Department of Physics, Tokyo Institute of Technology, Tokyo, Japan*
‡*TIES, Tokyo Institute of Technology, Tokyo, Japan*

E-mail: murakami@stat.phys.titech.ac.jp

Abstract

Based on the similarity between the chiral nanotube and the classical solenoid, we study chiral transport along the circumferential direction in a carbon nanotube. We calculate the chiral conductivity, representing a circumferential current induced by an electric field along the nanotube axis for various chiralities of carbon nanotubes. We find that the chiral conductivity in a chiral nanotube is in general non zero, and oscillates as a function of the Fermi energy. This oscillating behavior is attributed to the subband structure of the nanotubes and the warping of the Fermi surfaces.

Keywords

carbon nanotube, chiral transport, Edelstein effect, kinetic magnetoelectric effect

Introduction

Carbon nanotubes[1,2] have been attracting much interest for their unique properties and for their possibilities of applications for electronic devices, such as a field-emission display[3] and nanocomposite materials,[4] nanosensors.[5] Its novel transport properties has been revealed experimentally. For example, quantized conductance is measured,[6] and the ballistic conduction for both single[7] and multi-wall[8] carbon nanotubes are reported. Theoretically, a carbon nanotube can be either a metal or a semiconductor, depending on its chirality. This property is understood from the band structure of a graphene and periodic boundary conditions along the circumference direction. Because of the singular band structure and unique structure of a carbon nanotube, its transport properties are expected to be intriguing.[9–12]

In a chiral carbon nanotube, lower crystallographic symmetry allows chiral transport, i.e. a current in the circumferential direction induced by an electric field along the tube. Namely, when carriers are doped, an electric current along the tube axis induces a current around the tube. In a previous study, the chiral transport along the circumferential direction has been suggested in a BC_2N nanotube theoretically,[9] although the BC_2N nanotube has not been fabricated yet.[13] In Ref.,[9] both first-principles and tight-binding calculations are performed for the BC_2N nanotube, and they predicted that an electric field in BC_2N nanotube induces chiral transport, analogous to a solenoid. In Ref.,[14] the chiral conductivity is calculated for a BC_2N nanotube and a carbon nanotube and is shown to be non-zero. Here dependence on the chirality and on the doping are not explicitly shown. For the BN nanotube, the dynamical current directing the chiral shift has been calculated. However, the dependence on the chiral angle and the electronic concentration has not been studied.[15] Furthermore, chiral current is investigated for metallic carbon nanotubes[16] and stretched carbon nanotubes.[17] Experimental detection of the chiral current is also proposed.[18] The oscillation of the chiral currents

in a carbon nanotube as a function of the Fermi energy is reported, in which the giant magnetization is expected.[19] Moreover, chiral transport in three-dimensional chiral crystals has been also proposed recently,[20,21] as well as in three-dimensional topological insulators[22] and in two-dimensional surface and interfaces without inversion symmetry.[23]

In the present paper, we study dependence of the chiral current on the chirality of the carbon nanotubes. We calculate the chiral conductivity in carbon nanotubes, which is given by the ratio between the applied electric field along the nanotube axis and the induced current around the tube. As a function of the Fermi energy, the chiral conductivity is shown to oscillate with kinks. ThMoreover, its sign depends on $m-n$ modulo 3, where (m,n) is the chirality of the nanotube. This singular behavior is interpreted in terms of the subband structure of the nanotube, and warping of the Fermi surfaces is crucial here. Thus, it shows that the carbon nanotube is a unique stage for chiral transport, where chiral nature can be controlled in a unique way out of the same structure.

We first consider symmetry requirements to have chiral transport. When a current J flows along the tube axis, a chiral current is induced and a magnetization M along the tube will be induced. Thus the chiral response within the linear response is described as $M = CJ$ with constant C, and J being the current along the tube axis. This response is called kinetic magnetoelectric effect and orbital Edelstein effect,[20,21,24–32] and has been studied in the three-dimensional bulk metals[20,21]and in topological insulators.[22] This effect is an orbital analog of the spin Edelstein effect.[33–35] We will see in the following that the carbon nanotubes are special in that it contains various structures with various chiralities, based on the same two-dimensional graphene sheet. Then we can see that the system should simultaneously break three types of symmetries: (i) inversion symmetry, (ii) mirror symmetry with respect to the plane perpendicular to the tube axis, and (iii) mirror symmetry with respect to the plane including the tube axis, in order to realize chiral transport induced by a current along the tube. The response coefficient C vanishes when the system is invariant under either of these operations. In the three types of carbon nanotubes, i.e. armchair, zigzag and chiral ones, the symmetries are different as summarized in Table 1. We see that only chiral nanotubes break all the three types of symmetries. in the same way as in classical solenoids. Thus, chiral carbon nanotubes are candidates for a chiral transport, similar to a classical solenoid. We note that in some three-dimensional chiral materials, similar response has been discussed. In carbon nanotubes, we will see that based on a same bulk band structure of graphene, one can have varieties of chiral structures, and we can systematically study various chiral effects.

Table 1: Symmetries of three types of the carbon nanotubes. (i) inversion symmetry, (ii) mirror symmetry w.r.t. the plane including the tube axis, and (iii) mirror symmetry w.r.t the plane perpendicular to the tube axis.

	(i)	(ii)	(iii)
armchair	✓	✓	✓
zigzag	✓	✓	✓
chiral			

We here explain the chirality of the the carbon nanotube. Figures 1(a)(b) show the chiral vector $\mathbf{C}_h$ and the translational vector $\mathbf{T}$ for the chirality $(4,2)$. The chiral vector $\mathbf{C}_h$ is a translation vector in graphene, which constitutes the perimeter of the nanotube, The chiral vector $\mathbf{C}_h$ is written as $\mathbf{C}_h = \overrightarrow{\mathrm{OA}} = n\mathbf{a}_1 + m\mathbf{a}_2$, with integers m and n, where $\mathbf{a}_1 = a(1,0)$ and $\mathbf{a}_2 = a(1/2, \sqrt{3}/2)$ are translation vectors in graphene with lattice constant $a = 0.246$[nm].[36–38] Chirality of the carbon nanotube is then labeled by index (n,m). The vector $\mathbf{T}$, which is a primitive translation vector of the nanotube, is expressed as

$\mathbf{T} = \overrightarrow{\mathrm{OB}} = t_1\mathbf{a}_1 + t_2\mathbf{a}_2$ with $t_1 = -(2m+n)/d_R$, $t_2 = (2n+m)/d_R$ and d_R is the least common multiple of $2m+n$ and $2n+m$. The number of hexagon N, contained in unit cell described by the rectangle spanned by $\mathbf{C}_h$ and $\mathbf{T}$ in Fig. 1(a) is given by $N = 2(n^2+m^2+nm)/d_R$. The chiral angle θ_c, which is an angle between

$\mathbf{C}_h$ and $\mathbf{a}_1$, is given as $\theta_c = \tan^{-1}[\sqrt{3}m/(2n+m)]$. The zigzag, armchair and chiral carbon nanotubes can be distinguished by the chiral angle. The chiral angle is given by $\theta_c = 0, \pi/3$, $\theta_c = \pi/6$ and θ_c ($\neq 0, \pi/3, \pi/6$), for zigzag, armchair and chiral carbon nanotubes, respectively.

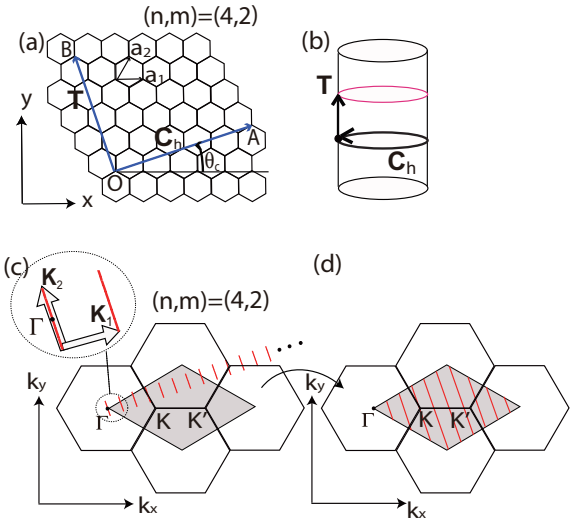


Figure 1: Structure of carbon nanotubes and their wavevectors. (a) Chiral vector $\mathbf{C}_h$ and the translational vector T for a carbon nanotube. (a) illustrates the case with the chirality (4,2). (b) The vectors $\mathbf{C}_h$ and $\mathbf{T}$ in the nanotube. (c) First Brillouin-zone for the (4,2) carbon nanotube is represented in blue. The gray hexagon represents the first Brillouin zone in graphene. The wavevector along the $\mathbf{K}_2$ is quantized, which is shown as a set of short segments shown in red. For convenience, we re-express the allowed wavevectors in (d) as a set of parallel segments inside the Brillouin zone of the graphene.

In the carbon nanotube, the wave number $\mathbf{k}$ along the circumferential direction is quantized.[36–38] Namely, the wave vector in the carbon nanotube is expaned in terms of $\mathbf{K}_1$ and $\mathbf{K}_2$ as

$$\mathbf{k} = k_1\mathbf{K}_1 + k_2\frac{\mathbf{K_2}}{|\mathbf{K_2}|}, \tag{1}$$

with k_1 quantized as

$$k_1 = 0, 1, 2, \cdots, N-1, -\pi/|\mathbf{T}| \leq k_2 < \pi/|\mathbf{T}|. \tag{2}$$

$\mathbf{K}_1$ and $\mathbf{K}_2$ are the reciprocal vectors of the carbon nanotube corresponding to $\mathbf{T}$ and $\mathbf{C}_h$, respectively, satisfying

$$\mathbf{C}_h\cdot\mathbf{K}_1 = 2\pi, \mathbf{C}_h\cdot\mathbf{K}_2 = 0, \mathbf{T}\cdot\mathbf{K}_1 = 0, \mathbf{T}\cdot\mathbf{K}_2 = 2\pi. \tag{3}$$

Namely, $\mathbf{K}_1$ and $\mathbf{K}_2$ are given by $\mathbf{K}_1 = (-t_2\mathbf{b}_1 + t_1\mathbf{b}_2)/N$ and $\mathbf{K}_2 = (m\mathbf{b}_1 - n\mathbf{b}_2)/N$, with $\mathbf{b}_1 = 2\pi(1, 1//\sqrt{3})$ and $\mathbf{b}_2 = (0, 4\pi/\sqrt{3})$. As an example, the first Brillouin zone of the carbon nanotube for the chirality $(4, 2)$ is shown in blue in Fig. 1(c).

The energy dispersion in the carbon nanotube can be described from that in graphene. Namely, the energy band in the carbon naotube is given by that in graphene with the wave vector quantized along the $\mathbf{K}_1$ direction. In this paper, we use the tight-binding model with a nearest-neighbor hopping,[9,39–41]

$$H = -\sum_{\langle i,j\rangle} t a_i^\dagger a_j, \tag{4}$$

where t is the hopping between the sites i and j, and $\langle\cdots\rangle$ means a summation over nearest-neighbor sites, with hopping integral $t \sim 3.0$eV for the tight-binding model. The energy dispersion in this system is given by

$$E_{\mathbf{k}}^{\pm} = \pm t\sqrt{1 + 4\cos^2\frac{ak_x}{2} + 4\cos\frac{ak_x}{2}\cos\frac{ak_y}{2}} \tag{5}$$

Here, we note that the energy dispersion is exactly the same as that in graphene, except the fact that the wave number is discretized in the carbon nanotube. The Fermi energy is set at $E_F = 0$. It is known that the carbon nanotube is metallic when the wave vector crosses the Dirac points at K and K' points in graphene which corresponds to $(n-m) \equiv 0 \pmod 3$, and semiconducting for the other chiralities.[11]

Results and discussion

We calculate the chiral conductivity when an electronic field is applied along the axis. With the Boltzmann transport equation, the conduc-

tivity is given by

$$\sigma_{ij} = -e^2 \sum_{\mathbf{k}}^{\mathrm{BZ}} v_i v_j \frac{\partial f(E_{\mathbf{k}})}{\partial E_k} \tau, \ i,j = x,y, \quad (6)$$

where $f(E_{\mathbf{k}})$ is the Fermi distribution function, and the summation is taken over the allowed wavevectors within the Brillouin zone (BZ), $\mathbf{v} = (v_x, v_y)$ is the velocity of an electron, and τ is the relaxation time assumed to be constant. By using $v_i = \hbar^{-1} dE_{\mathbf{k}}/dk_i$ and partial integration, at zero temperature, we obtain

$$\sigma_{ij} = \frac{e^2\tau}{\hbar^2} \sum_{k_1} \int dk_2 \frac{\partial^2 E^-_{\mathbf{k}}}{\partial k_i \partial k_j}, \quad (7)$$

which is a convenient form for numerical calculation. The sum over k_1 in eq. (7) is taken over the discretized wave vector k_1 in eq. (1).

We can calculate the chiral conductivity σ_{12} from σ_{xx}, σ_{xy} and σ_{yy} in eq. (7), by rotating the coordinate axes from x, y to $1, 2$ bythe angle θ_c. As a result, the chiral conductivity σ_{12} is obtained as

$$\begin{pmatrix} \sigma_{11} & \sigma_{12} \\ \sigma_{21} & \sigma_{22} \end{pmatrix} = \begin{pmatrix} \cos\theta_c & \sin\theta_c \\ -\sin\theta_c & \cos\theta_c \end{pmatrix} \times \begin{pmatrix} \sigma_{xx} & \sigma_{xy} \\ \sigma_{yx} & \sigma_{yy} \end{pmatrix} \begin{pmatrix} \cos\theta_c & -\sin\theta_c \\ \sin\theta_c & \cos\theta_c \end{pmatrix}, \quad (8)$$

where 1 and 2 represent the circumferential direction and the direction along the tube, respectively. We calculate the chiral conductivity σ_{12} by varying two parameters, the chirality (n, m) and the electronic concentration n_i. Because the band dispersion depends on chirality, the Fermi level is numerically determined for an electronic concentration n_i for each carbon nanotube.

Figures 2 (a) and (b) shows the chiral conductivity σ_{12} as a function of the chiral angle for the electronic concentration $n_i = 0.001$, measured from the undoped value. We set the chirality as $(8, m)$ in (a) and $(15, m)$ in (b), where integer m is changed from 0 to 8. Generally, the sign of the chiral conductivity σ_{12} depends on m through the value $(n - m) \equiv 0, 1, 2 \pmod 3$. Namely, for $(n - m) \equiv 1$ (2) (mod 3), the sign of σ_{12} is positive (negative). For $(n - m) \equiv 0 \pmod 3$ when the carbon nanotube becomes metallic, σ_{12} is almost zero. We note that σ_{12} becomes zero for $m = 0$ because the carbon nanotube is of the armchair type and chiral transport is prohibited by symmetry. Furthermore, $|\sigma_{12}|$ tends to become larger as the chiral angle increases, with an exception of $m = 5, 10$ for $n = 15$.

We found that σ_{12} tend to become larger as the integers m and n in the chirality (m, n) become larger in general, by calculating also for the chiralities $(4, m)$, $(12, m)$, $(20, m)$ and $(30, m)$, although not shown here. This is because the contribution from the Fermi surfaces to σ_{12} becomes larger for large chirality. The density of states on the Fermi level increases as chirality increases, with some exceptions with accidental local minima of σ_{12} such as those for $m = 5, 10$ in Fig. 2(b). We interpret these remarkable dependences of σ_{12} on chirality in terms of the warping of the Fermi surfaces. For large doping, the warping effect is prominent and the contributions to σ_{12} do not perfectly cancel each other in metallic carbon nanotube, as we discuss later.

Figures 2(c) and (d) shows σ_{12} as a function of electronic concentration n_i for $0 \leq n_i \leq 0.2$ for the chiralities (a) $(8, 6)$ and (b) $(20, 16)$. Generally, σ_{12} oscillates as a function of n_i, with sharp kinks where σ_{12} changes between an increasing and a decreasing function of n_i. As n_i becomes even larger and approaches 1, which is not realistic but is studied only for a theoretical interest, the chiral conductivity converges to zero, because electrons occupy all the bands in the model, giving no carriers in the hole picture.

To explain the oscillation of σ_{12}, we analyze the dependence of σ_{12} on n_i in the $(8, 6)$ carbon nanotube for $0 \leq n_i \leq 0.2$ in Fig. 2 (c). As an example, in Fig. 3(a) we show the Fermi surface at $n_i = 0.03$, where σ_{12} monotonically increases. The rhombus in the figure is the unit cell for the reciprocal space of graphene, which is equivalent to the first Brillouin zone. The wavevector $\mathbf{k}$ is discretized along the $\mathbf{K}_1$ direction (see eq. (1)), shown as the parallel lines, giving rise to subband structures. We label each subband by the value of the integer k_1, and they

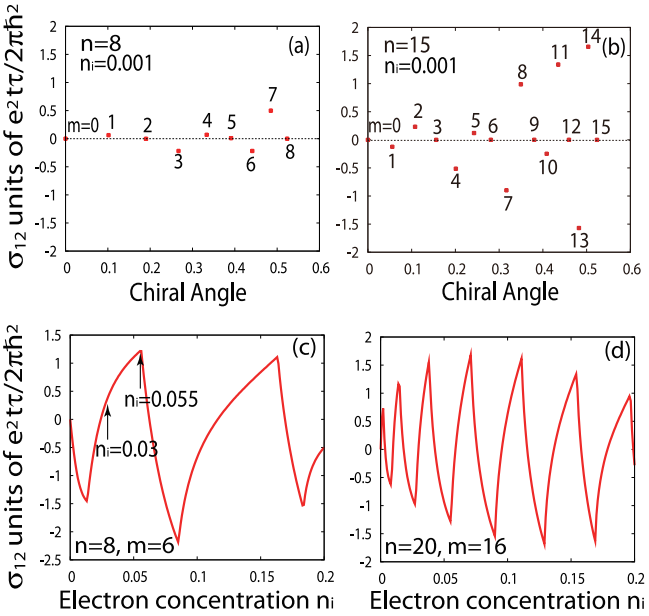


Figure 2: Chiral conductivity σ_{12}. (a)(b) Chiral conductivity as a function of the chiral angle for $n_i = 0.001$. The chirality is set as (a) $(8, m)$ with $m = 0, 1, \cdots, 8$ and (b) $(15, m)$ with $m = 0, 1, \cdots, 15$. (c)(d) Chiral conductivity as a function of the electron concentration for (c) (8,6) and (d) (20,16) nanotubes.

are shown as the indices from 5 to 9 for the subbands near the Fermi level. There are two Fermi surfaces, near the K and the K' points for the graphene. At $n_i = 0.03$, the Fermi level crosses only the 7th and 8th lines. The chiral conductivity σ_{12} in eq. (6) is attributed to the states at the Fermi energy. Here we focus on the Fermi surface near the K point, because the contribution from the states near the K point and that near the K' point are the same by the time-reversal symmetry. The states on the Fermi level near the K point are represented by four intersection points between the Fermi surface and the allowed wavevectors specified by the parallel lines. On the other hand, for $n_i = 0.055$, where the chiral conductivity σ_{12} shows a peak in Fig. 2 (c), the Fermi surface is illustrated in Fig. 3 (a). In addition to the four intersection points on the 7th and the 8th lines in Fig. 3 (a), the Fermi surface and the 6th line come in contact with each other in this case. To see how each band contributes to the chiral conductivity σ_{12}, we show in Fig. 3 (c) the contributions to σ_{12} from each subband as a function of n_i. We can see the negative contribution from the 6th band in Fig. 3 (c) appears for $n_i > 0.055$. Therefore, the sharp kink of σ_{12} at $n_i = 0.055$ is attributed to the negative contribution of the 6th band to σ_{12} for $n_i > 0.055$. As the electron concentration increases, the Fermi surface crosses the 7th, 8th, 6th, 9th and 5th bands consecutively, and they contribute to the chiral conductivity with various signs. This corresponds to the points of the sharp kinks in Fig. 2 (c). Besides, the signs of the contributions changes alternately in the order, 7th, 8th, 6th, 9th and 5th, which explains the oscillation of σ_{12} as a function of n_i.

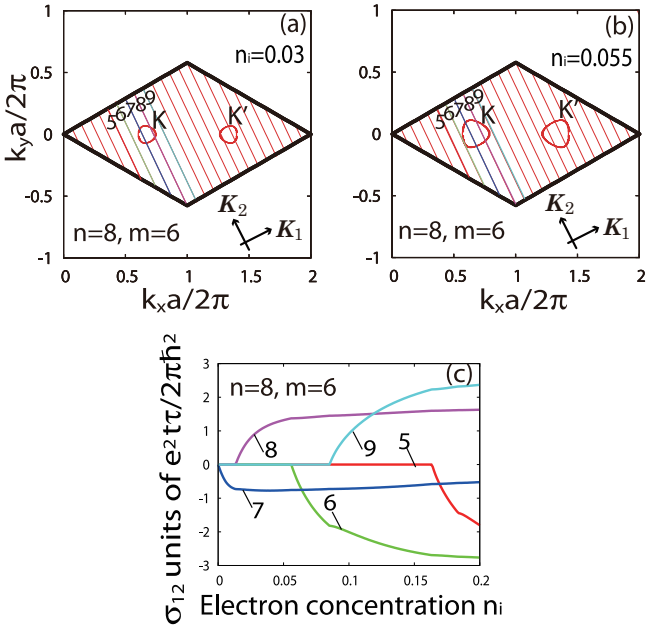


Figure 3: Singular behaviors of chiral condiuctivities from subband contributions. The Fermi surface of the $(8, 6)$ carbon nanotube is shown for (a) $n_i = 0.03$ and (b) $n_i = 0.055$ in the first Brillouin zone in graphene. The lines are the discretized wave vectors of carbon nanotubes. The indexes 5-9 are subband indices showing the values of k_1. (c) The contribution from the l-th band ($l = 5, 6, 7, 8, 9$) to σ_{12} as a function of the electronic concentration n_i for the chirality $(8, 6)$. Each color and number correspond to those in (a) and (b).

Figure 2 (d) shows n_i dependence of σ_{12} for the chirality $(20, 16)$. The range of the oscillation is larger, and the period of the oscillation is smaller than those for the chirality $(8, 6)$.

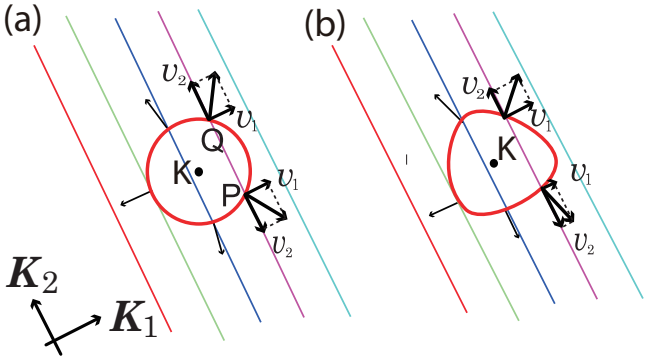


Figure 4: Effect of the warping of the the Fermi surface onto the chiral conductivities. The Fermi surface (a) without and (b) with warping near the K point in graphene. The lines describe the subbands of the carbon nanotube. The arrows normal to the Fermi surface denote the Fermi velocity, which can be decomposed into the circumferential velocity v_1 and the velocity along the tube v_2.

To understand the reason for the singular behavior of σ_{12}, we first assume the band structure around the K point to be a perfect Dirac cone with perfect linear dispersion $E_{\mathbf{k}} = \gamma|\mathbf{k} - \mathbf{k}_0|$ where γ is a constant, and $\mathbf{k}_0$ is either the K or K' point. Then σ_{12} is completely zero for any chiralities and the electronic concentrations. Since the linear dispersion $E_{\mathbf{k}} = \gamma|\mathbf{k}-\mathbf{k}_0|$ makes the Fermi surface to be a circle without warping, there are always a pair of Fermi points in the same subband, where the values of v_1 are the same while the signs of v_2 are opposite (the points P and Q in Fig. 4 (a)). Their contributions to σ_{12} in eq. (6) completely cancels each other because of symmetry. In reality, the Fermi surfaces in carbon nanotubes are distorted from a circle and have a warping (Fig. 4 (b)). For the Fermi surface with the warping, the chiral conductivity has a nonzero value in general, because the contributions from the Fermi points do not necessarily cancel each other.

For $n - m \equiv 0 \pmod 3$, one of the subbands crosses the Dirac point in graphene. In this case, the contributions cancel each other almost completely for the low electronic concentration such as $n_i = 0.001$, because the Fermi surface is almost symmetric with respect to the subband line going across the Dirac point. However, the contribution does not vanish completely each other for a higher electronic concentration, because of the large warping of the Fermi surface.

We now estimate the value of the current flowing along the circumferential direction. When the electric field is applied along the axis, the current per unit length along the circumferential direction j_1 is given by

$$j_1 = \frac{\sigma_{12}}{\sigma_{22}} \frac{I_2}{2\pi R}, \tag{9}$$

where I_2 is the current along the nanotube, and R is the radius of the carbon nanotube. We note that σ_{22} is the longitudinal conductivity along the tube axis, calculated from eq. (8). In Fig. 5(a), we show the comparison of σ_{22} and σ_{12} in the $(8, 6)$ carbon nanotube, where the diameter is $R = 0.47$nm. σ_{22} increases with some oscillations as n_i increases. σ_{22} shows a moderate kink at the electronic concentrations where σ_{12} shows sharp peaks and dips. This is becasue new subbands begin to contribute to σ_{12} andσ_{22}, as we increase the concentration, as we have seen in this paper. In Fig. 5(b), we show the ratio between σ_{22} and σ_{12}, which represents a dimensionless figure of merit for the chiral transport. We note that the ratio becomes largest at a very low concentration, and that it oscillates, converging to zero for larger n_i because σ_{22} increases rapidly as the Fermi level increases. The positions of the peaks of the oscillation correspond to that of σ_{12} and σ_{22}. For a very low concentration region, the ratio takes a value ~ -0.15 in this case, and becomes zero at $n_i = 0$. For the $(8, 6)$ nanotube, the maximum current which can be applied to the carbon nanotube is $I_1^{\max} \times S = 6.6 \times 10^{-8}$A,[42] with the cross section of the $(8, 6)$ nanotube $S = 6.6 \times 10^{-17}\text{cm}^2$. For $\sigma_{12}/\sigma_{22} \sim -1.5$, j_1 is $j_1 = -3.5$A/cm from eq. (9), corresponding to 4.4 gauss. The (orbital) magnetization per unit length of the nanotube is estimated as $M = j_2 S = -0.23 \times 10^{-15}\text{A} \cdot \text{cm}$.

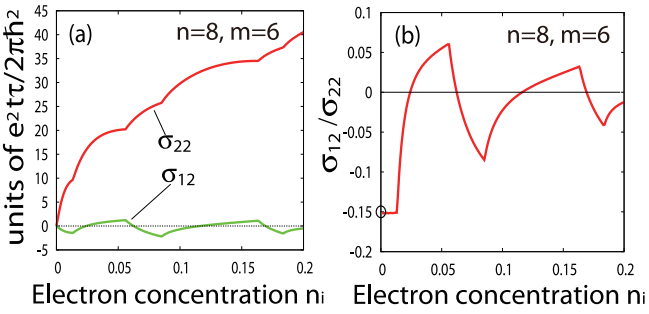


Figure 5: The longitudinal conductivity σ_{22} and the chiral conductivity σ_{12}. (a) σ_{12} and σ_{22} as functions of n_i in the $(8,6)$ nanotube. (b) σ_{12}/σ_{22} as a function of n_i in the $(8,6)$ nanotube.

Concluding remarks

In conclusion, we studied chiral transport in carbon nanotubes. We calculated the chiral conductivity by using the tight-binding model and the Boltzmann transport equation for the electric field applied along the axis of the carbon nanotube. We found that the chiral conductivity σ_{12} is nonzero for semiconducting chiral carbon nanotubes with doping. For a constant electronic concentration, its sign alternately changes as the chiral angle increases, and it becomes positive, negative and zero when for the cases with $n - m \equiv 1, 2, 0 (\mathrm{mod} 3)$, respectively. As a function of the electron concentration, σ_{12} oscillates. This is attributed to the different signs of the contributions from the individual subbands to σ_{12}. As the electronic concentration increases, the Fermi surface crosses the subbands with positive and negative contributions to σ_{12}, giving rise to a peculiar oscillatory dependence on the concentration. Finally, we have estimated the value of chiral current and magnetization induced by the chiral current.

This kind of chiral transport has been also studied in bulk metals and topological insulators in three dimensions. For example, in tellurium, this chiral transport has been evaluated by *ab initio* calculation[28] and a related experiment on current-induced magnetization has been performed.[26] Tellurium hss left-handed and right-handed crystals, which consist of one-dimensional chains in shapes of helices, and one can see its analogy with a classical solenoid easily. On the other hand, in chiral nanotubes, its chirality is not fixed but can switch between both directions by changing an electron concentration.

This effect induces an orbital magnetization in carbon nanotubes, and through the spin-orbit coupling it might also lead to spin magnetization, which might be one route to induce the chirality-induced spin selectivity (CISS) effect.[43–47]

Notes

The authors declare no competing financial interest.

Acknowledgement This work was supported by JSPS KAKENHI Grants No. JP30578216, No. 23740236, No.26287062, and No. 18H03678, by the JSPS-EPSRC Core-to-Core program "Oxide Superspin", by MEXT KAKENHI Grants No. 25103709, and No.26103006, and by Elements strategy Initiative to Form Core Research Center (TIES), from MEXT Grant Number JPMXP0112101001.

References

(1) Iijima, S. Helical microtubules of graphitic carbon. *Nature* **1991**, *354*, 56–58.

(2) Iijima, S.; Ichihashi, T. Single-shell carbon nanotubes of 1-nm diameter. *Nature* **1993**, *363*, 603–605.

(3) Liu, Z.; Jiao, L.; Yao, Y.; Xian, X.; Zhang, J. Aligned, Ultralong Single-Walled Carbon Nanotubes: From Synthesis, Sorting, to Electronic Devices. *Advanced Materials* **2010**, *22*, 2285–2310.

(4) Byrne, M. T.; Gun'ko, Y. K. Recent Advances in Research on Carbon Nanotube-Polymer Composites. *Advanced Materials* **2010**, *22*, 1672–1688.

(5) Allen, B.-L.; Kichambare, P.-D.; Star, A. Carbon Nanotube Field-Effect-Transistor-Based Biosensors. *Advanced Materials* **2007**, *19*, 1439–1451.

(6) Kong, J.; Yenilmez, E.; Tombler, T. W.; Kim, W.; Dai, H.; Laughlin, R. B.; Liu, L.; Jayanthi, C. S.; Wu, S. Y. Quantum Interference and Ballistic Transmission in Nanotube Electron Waveguides. *Phys. Rev. Lett.* **2001**, *87*, 106801.

(7) Javey, A.; Guo, J.; Wang, Q.; Lundstrom, M.; Dai, H. Ballistic carbon nanotube field-effect transistors. *Nature* **2003**, *424*, 654–657.

(8) Berger, Y., C.and Yi; Wang, Z. L.; de Heer, W. A. Multiwalled carbon nanotubes are ballistic conductors at room temperature. *Appl Phys A* **2002**, *74*, 363–365.

(9) Miyamoto, Y.; Rubio, A.; Cohen, M. L.; Louie, S. G. Chiral tubules of hexagonal BC_2N. *Phys. Rev. B* **1994**, *50*, 4976–4979.

(10) Ando, T. Theory of transport in carbon nanotubes. *Semiconductor Science and Technology* **2000**, *15*, R13–R27.

(11) Ando, T.; Nakanishi, T. Impurity Scattering in Carbon Nanotubes - Absence of Back Scattering -. *Journal of the Physical Society of Japan* **1998**, *67*, 1704–1713.

(12) Nakanishi, T.; Ando, T. Numerical Study of Impurity Scattering in Carbon Nanotubes. *Journal of the Physical Society of Japan* **1999**, *68*, 561–566.

(13) Ayala, P.; Arenal, R.; Loiseau, A.; Rubio, A.; Pichler, T. The physical and chemical properties of heteronanotubes. *Rev. Mod. Phys.* **2010**, *82*, 1843–1885.

(14) Miyamoto, Y.; Louie, S. G.; Cohen, M. L. Chiral Conductivities of Nanotubes. *Phys. Rev. Lett.* **1996**, *76*, 2121–2124.

(15) Král, P.; Mele, E. J.; Tománek, D. Photogalvanic Effects in Heteropolar Nanotubes. *Phys. Rev. Lett.* **2000**, *85*, 1512–1515.

(16) Tsuji, N.; Takajo, S.; Aoki, H. Large orbital magnetic moments in carbon nanotubes generated by resonant transport. *Phys. Rev. B* **2007**, *75*, 153406.

(17) Miyamoto, Y. Mechanically stretched carbon nanotubes: Induction of chiral current. *Phys. Rev. B* **1996**, *54*, R11149–R11152.

(18) Miyamoto, Y.; Rubio, A.; Louie, S. G.; Cohen, M. L. Self-inductance of chiral conducting nanotubes. *Phys. Rev. B* **1999**, *60*, 13885–13889.

(19) Lambert, C. J.; Bailey, S. W. D.; Cserti, J. Oscillating chiral currents in nanotubes: A route to nanoscale magnetic test tubes. *Phys. Rev. B* **2008**, *78*, 233405.

(20) Yoda, T.; Yokoyama, T.; Murakami, S. Current-induced Orbital and Spin Magnetizations in Crystals with Helical Structure. *Sci. Rep.* **2015**, *5*, 12024.

(21) Yoda, T.; Yokoyama, T.; Murakami, S. Orbital Edelstein Effect as a Condensed-Matter Analog of Solenoids. *Nano Letters* **2018**, *18*, 916–920, PMID: 29373028.

(22) Osumi, K.; Zhang, T.; Murakami, S. Orbital Edelstein effect in topological insulators. 2021; arXiv:2101.01869.

(23) Hara, D.; Bahramy, M. S.; Murakami, S. Current-induced orbital magnetization in systems without inversion symmetry. *Phys. Rev. B* **2020**, *102*, 184404.

(24) Shalygin, V. A.; Sofronov, A. N.; Vorob'ev, L. E.; Farbshtein, I. I. Current-induced spin polarization of holes in tellurium. *Physics of the Solid State* **2012**, *54*, 2362–2373.

(25) Koretsune, T.; Arita, R.; Aoki, H. Magneto-orbital effect without spin-orbit interactions in a noncentrosymmetric zeolite-templated carbon structure. *Phys. Rev. B* **2012**, *86*, 125207.

(26) Furukawa, T.; Shimokawa, Y.; Kobayashi, K.; Itou, T. Observation of current-induced bulk magnetization in elemental tellurium. *Nat. Commun.* **2017**, *8*, 954.

(27) Zhong, S.; Moore, J. E.; Souza, I. Gyrotropic Magnetic Effect and the Magnetic Moment on the Fermi Surface. *Phys. Rev. Lett.* **2016**, *116*, 077201.

(28) Tsirkin, S. S.; Puente, P. A.; Souza, I. Gyrotropic effects in trigonal tellurium studied from first principles. *Phys. Rev. B* **2018**, *97*, 035158.

(29) Furukawa, T.; Watanabe, Y.; Ogasawara, N.; Kobayashi, K.; Itou, T. Chirality-Induced Electrical Generation of Magnetism in Nonmagnetic Elemental Tellurium. 2020; arXiv:2010.09210.

(30) Rou, J.; Şahin, C.; Ma, J.; Pesin, D. A. Kinetic orbital moments and nonlocal transport in disordered metals with nontrivial band geometry. *Phys. Rev. B* **2017**, *96*, 035120.

(31) Şahin, C.; Rou, J.; Ma, J.; Pesin, D. A. Pancharatnam-Berry phase and kinetic magnetoelectric effect in trigonal tellurium. *Phys. Rev. B* **2018**, *97*, 205206.

(32) Hara, D.; Bahramy, M. S.; Murakami, S. Current-induced orbital magnetization in systems without inversion symmetry. *Phys. Rev. B* **2020**, *102*, 184404.

(33) Edelstein, V. Spin polarization of conduction electrons induced by electric current in two-dimensional asymmetric electron systems. *Solid State Commun.* **1990**, *73*, 233–235.

(34) Ivchenko, E. L.; Pikus, G. E. New photogalvanic effect in gyrotropic crystals. *ZhETF Pisma Redaktsiiu* **1978**, *27*, 640.

(35) Levitov, L. Nazarov Yu. V. and Eliashberg G. M. *Sov. Phys. JETP* **1985**, *61*, 133.

(36) Saito, R.; Dresselhaus, G.; Dresselhaus, M. S. *Physical Properties of Carbon Nanotubes*; Published by Imperial College Press and distributed by World Scientific Publishing Co., 1998.

(37) Dresselhaus, M.; Dresselhaus, G.; Eklund, P. In *Science of Fullerenes and Carbon Nanotubes*; Dresselhaus, M., Dresselhaus, G., Eklund, P., Eds.; Academic Press: San Diego, 1996.

(38) Ajiki, H.; Ando, T. Electronic States of Carbon Nanotubes. *Journal of the Physical Society of Japan* **1993**, *62*, 1255–1266.

(39) Hamada, N.; Sawada, S.-i.; Oshiyama, A. New one-dimensional conductors: Graphitic microtubules. *Phys. Rev. Lett.* **1992**, *68*, 1579–1581.

(40) Saito, R.; Fujita, M.; Dresselhaus, G.; Dresselhaus, M. S. Electronic structure of graphene tubules based on C_{60}. *Phys. Rev. B* **1992**, *46*, 1804–1811.

(41) Saito, R.; Fujita, M.; Dresselhaus, G.; Dresselhaus, M. S. Electronic structure of chiral graphene tubules. *Applied Physics Letters* **1992**, *60*, 2204–2206.

(42) Dekker, C. Carbon Nanotubes as Molecular Quantum Wires. *Physics Today* **1999**, *52*, 22–28.

(43) Naaman, R.; Waldeck, D. H. Chiral-Induced Spin Selectivity Effect. *The Journal of Physical Chemistry Letters* **2012**, *3*, 2178–2187.

(44) Gohler, B.; Hamelbeck, V.; Markus, T. Z.; Kettner, M.; Hanne, G. F.; Vager, Z.; Naaman, R.; Zacharias, H. Spin Selectivity in Electron Transmission Through Self-Assembled Monolayers of Double-Stranded DNA. *Science* **2011**, *331*, 894–897.

(45) Kettner, M.; Maslyuk, V. V.; Nürenberg, D.; Seibel, J.; Gutierrez, R.; Cuniberti, G.; Ernst, K.-H.; Zacharias, H.

Chirality-Dependent Electron Spin Filtering by Molecular Monolayers of Helicenes. *The Journal of Physical Chemistry Letters* **2018**, *9*, 2025–2030.

(46) Bloom, B. P.; Kiran, V.; Varade, V.; Naaman, R.; Waldeck, D. H. Spin Selective Charge Transport through Cysteine Capped CdSe Quantum Dots. *Nano Letters* **2016**, *16*, 4583–4589.

(47) Dor, O. B.; Morali, N.; Yochelis, S.; Baczewski, L. T.; Paltiel, Y. Local Light-Induced Magnetization Using Nanodots and Chiral Molecules. *Nano Letters* **2014**, *14*, 6042–6049.